AMSI VACATIONRESEARCH SCHOLARSHIPS 2020–21

Get a Thirst for Research this Summer

Nanoscale sessile droplet shape prediction. Comparison between theory and experiment

Benjamin Babu

Supervised by Assoc. Prof. Bronwyn Hajek

Assoc. Prof. Marta Krasowska

University of South Australia

Vacation Research Scholarships are funded jointly by the Department of Education, Skills and Employment and the Australian Mathematical Sciences Institute.

Contents

1 Abstract

Nanoscale sessile droplets can be scanned using AFM (atomic force microscopy) to attain a topographic image of the droplet profile, however, there are some issues with using AFM including inaccuracies near the edge of the droplet and different interactions on each side. The Young-Laplace equation can be used to model droplets shapes that are in the macroscopic range and here we use it for droplets in the nanometer range. The main aims of the project are to predict the true droplet shape as well as to make a quantitative comparison between the theoretical and experimental measurements. The non-dimensionalised Young-Laplace equations were solved and the solutions were plotted with the experimental data points; the fit was found to be very good. A quantitative comparison was made using absolute and relative errors. As expected we found that the errors were high at the edge of the droplets and low at the apex of the droplets. In addition, the errors are significantly larger on one side than the other.

2 Introduction

When an oil droplet is flat on a surface, it will have a shape approximating a spherical cap. The circular edge of the droplet where the drop meets the flat surface is called the three-phase contact line as this is where the three phases meet, that is, where the flat solid surface, the liquid oil drop, and the surrounding water meet. The angle at which all three phases meet, the so-called contact angle, can be determined using the Young-Laplace equation which balances surface tension with the pressure difference across the droplet's interface [1]. This is a well-adapted approach for macroscopic (micron size and larger) droplets, however it becomes more complicated as the droplet's dimensions become smaller (in nanometre range). Atomic force microscopy (AFM) can study samples at the nanoscale performing three-dimensional topography. An AFM scans over a sample surface with a sharp tipped cantilever which deflects towards or away from the surface as it is brought closer. These deflections, which are caused by van der Waal's forces, are then detected by reflecting an incident laser beam off the cantilever; any deflections will cause directional changes of the reflected beam. These changes are tracked using a position-sensitive photo diode which can then be used for accurate topography/imaging [2].

However, there are two major problems associated with measuring droplets using AFM.

1. The AFM cannot obtain an accurate profile/height of the droplet's surface near the three-phase contact line, so the AFM image shows a curved or gradual join instead of a sharp corner. This is due to the fact that the cantilever's tip is not precisely a point, rather it has a small radius. The smaller the radius of the tip, the more accurate the imaging resolution [3].

2. The cantilever is on a slight angle as it moves over the surface. This means that it interacts differently with one side of the droplet to the other. AFM images show that the droplet is not symmetric, but rather, it is flatter on one side and steeper on the other [4].

This report will aim to make a quantitative comparison between the theoretical droplet shape obtained from

solving the Young-Laplace equation with experimental AFM measurements. In addition, we predict the true droplet shape at the contact phase line position/angle using the more accurate AFM measurements taken near the centre of the droplet.

3 Experimental Data

As described above, AFM measurements can be used to determine the profile of a small droplet on a flat substrate. Figure 1 shows experimental data for three such profiles of an oil droplet on a silicon substrate, submerged in water.

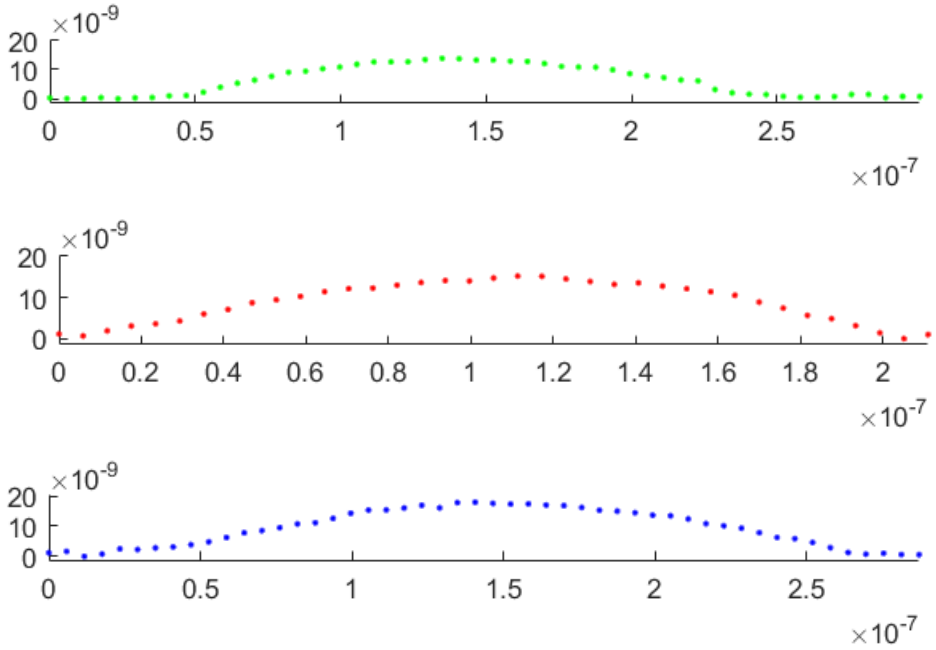

Figure 1: Experimental measurements of three different drop profiles

As discussed earlier, all the droplets do not seem to have a sharp contact angle, but rather, a smooth curve due to the challenges of using the AFM in the regions where the droplet height is very small. Upon further inspection, some points have non-zero height well beyond the extent of the drop which is an indication of possible errors. It can also be noticed that the profile near the drop edges is not always monotonic.

4 Modelling and the Young-Laplace equation

A schematic of the droplet is shown in Figure 2. The droplet surface is located at $(Z(S), R(S))$ where $Z(S)$ is the dimensional vertical distance downwards from the top of the droplet and $R(S)$ is the radial distance from the droplet centre. Both are functions of the arc length, S, from the top of the droplet. The angle between the

tangent to the droplet surface and the horizontal is given by $\theta(S)$. Note that θ will be the contact angle when $Z = h$ since h is the maximum height of the droplet. The volume of the droplet is given by $V(S)$ and will be equal to the total volume of the droplet when $Z = h$.

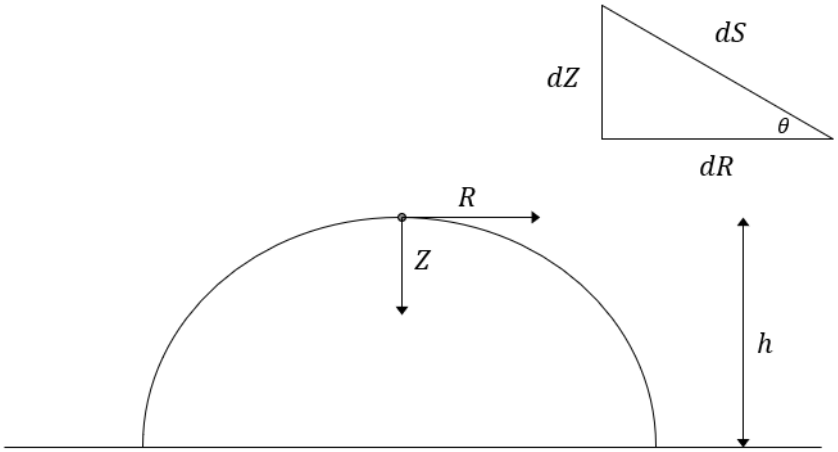

Figure 2: Schematic of a droplet and the coordinate system. The triangle represents an infinitesimal section of the arc length.

The co-ordinates describing the location of the drop profile and the angle between the tangent and the horizontal can be related by a system of differential equations known as the Young-Laplace equations. These equations are written as

$$\frac{dR}{dS} = \cos\theta \tag{1}$$

$$\frac{dZ}{dS} = \sin\theta \tag{2}$$

$$\frac{d\theta}{dS} = 2\kappa + \frac{\Delta\rho g}{\gamma} Z - \frac{\sin\theta}{R} \tag{3}$$

$$\frac{dV}{dS} = \pi R^2 h \sin\theta \tag{4}$$

where κ is the curvature of the interface of the top of the droplet, $\Delta\rho = \rho_{oil} - \rho_{water}$ is the difference in densities between the droplet and the surrounding fluid, γ is the interfacial tension of the oil-water surface, and g is gravity.

Equations (1) and (2) are derived using standard trigonometric relations and the right angle triangle in Figure 2. Equation (3) is obtained by balancing the Laplace pressure across the curvature of the interface with the inter-facial tension. Equation (4) is not needed to close the system, however, it serves as an auxiliary, and could be used should the volume be required. It is derived by taking infinitesimal horizontal slices of the droplet and by relating the volume of each slice to the arc length of the slice.

Before solving this system of differential equations, boundary conditions need to be established at the top of

the droplet, where $S = 0$,

$$R(0) = 0, \quad Z(0) = 0, \quad \theta(0) = 0, \quad V(0) = 0. \tag{5}$$

In addition,

$$\frac{\sin(\theta)}{R} = \kappa,$$

so that from Equation (3) we have,

$$\left.\frac{d\theta}{dS}\right|_{S=0} = \kappa. \tag{6}$$

5 Parameter values

The constant values of the parameters are as follows:

$$\begin{aligned} g &= 9.8 \quad \text{ms}^{-2} \\ \gamma &= 0.0162 \quad \text{Nm}^{-1} \\ \Delta\rho &= \rho_{oil} - \rho_{water} \\ &= 997 - 917 \\ &= 80 \quad \text{kgm}^{-3} \end{aligned}$$

The values for h and κ are unique to each droplet as each of them will a different volume, and consequently a different height and radius and thus, a different curvature. The values for these parameters can be found by fitting a circle to the accurate parts of the experimental data, i.e. those data points away from the droplet edge. The curvature κ can be found by finding the inverse of the radius of the spherical approximation of the droplet. Furthermore, the height h can be found by taking the difference between the absolute value of the y coordinate and the radius. The details are shown in Figure 3.

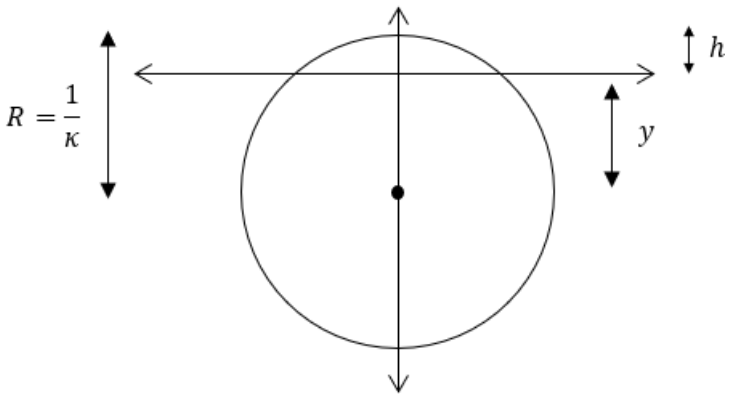

Figure 3: Schematic of fitting a circle to the experimental data

As mentioned above, the accurate experimental data points are those away from the edge of the droplet. Data higher than $\frac{1}{4}$ of the maximum height was used. Figure 4 shows the data points that were used in the spherical approximation.

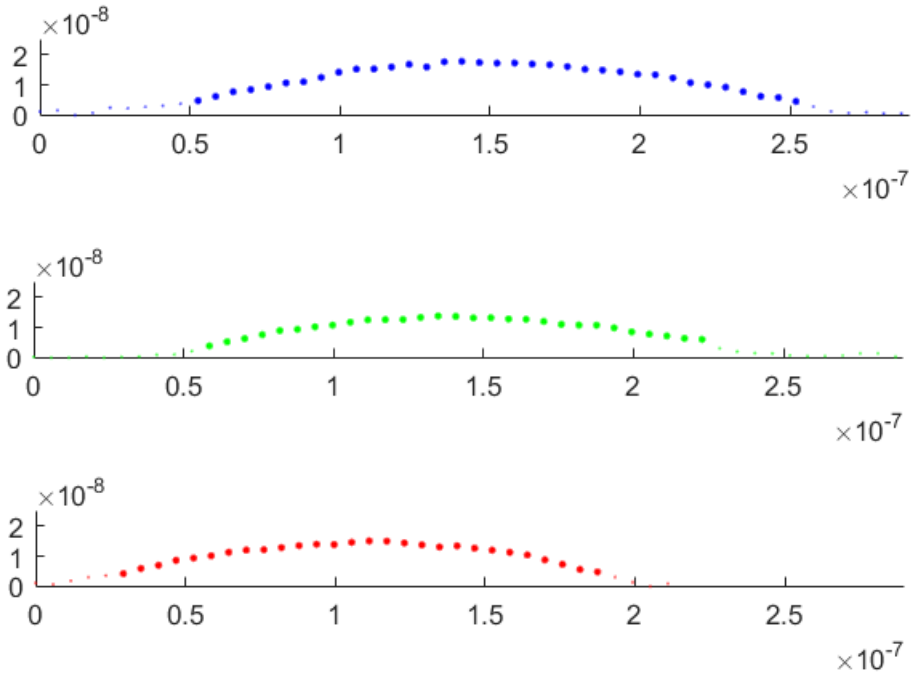

Figure 4: Three droplet profiles where the data points used in the spherical approximation are shown with a larger marker, while those too close to the droplet edge are shown with a small marker.

Using a community MATLAB function, a circle was fitted onto the data-sets which can be seen in Figure 5. Figure 5c suggests that the circle fits well, as the data points used in the fit all lie very close to the circle.

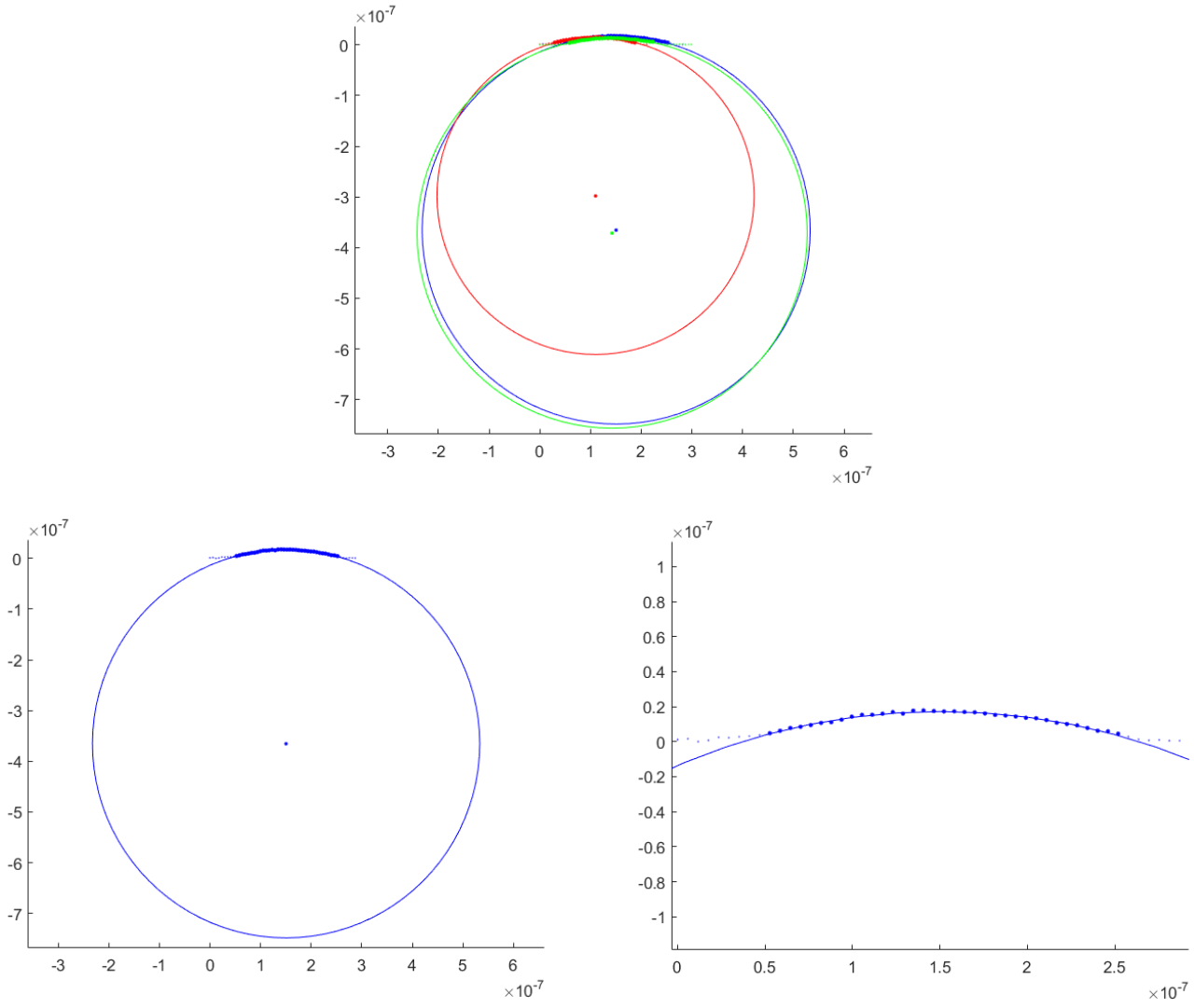

Figure 5: Fitting circle to the experimental data. (a) All three data sets with their respective approximate circles. The centre of each circle is also shown. (b) The fitted circle for the first data set. (c) Zoomed in view of the first data set and fit.

6 Non-dimensionalisation of the model

Non-dimensionalisation is the process of transforming a model into its dimensionless form by re-scaling variables. It makes solution and analysis easier by

1. reducing the number of fundamental parameters,
2. making the equations unit-less so that no scaling or unit issues will be present,
3. simplifying the model, making it easier to analyse.

To non-dimensionalise the Young-Laplace equations we introduce the non-dimensional variables $r = \frac{R}{h}$, $s = \frac{S}{h}$,

$z = \frac{Z}{h}$, and $v = \frac{V}{U}$ where U is a characteristic volume yet to be determined.

Non-dimensionalisation of equation (1)

Making use of the chain rule,

$$\begin{aligned} \frac{dR}{dS} &= \cos\theta, \\ \frac{d(hr)}{ds}\frac{ds}{d(hs)} &= \cos\theta, \\ \frac{h}{h}\frac{dr}{ds} &= \cos\theta, \end{aligned}$$

so that

$$\frac{dr}{ds} = \cos\theta. \tag{7}$$

Non-dimensionalisation of (2)

Substituting the new variables into equation (2) and making use of the chain rule,

$$\begin{aligned} \frac{dZ}{dS} &= \sin\theta, \\ \frac{d(hz)}{ds}\frac{ds}{d(hs)} &= \sin\theta, \\ \frac{h}{h}\frac{dz}{ds} &= \sin\theta, \\ \frac{dz}{ds} &= \sin\theta. \end{aligned} \tag{8}$$

Non-dimensionalisation of equation (3)

Substituting the new variables and making use of the chain rule in equation (3) gives

$$\begin{aligned} \frac{d\theta}{dS} &= 2\kappa + \frac{\Delta\rho g}{\gamma}Z - \frac{\sin(\theta)}{R}, \\ \frac{d\theta}{ds}\frac{ds}{d(hs)} &= 2\kappa + \frac{\Delta\rho g}{\gamma}hz - \frac{\sin(\theta)}{hr}, \\ \frac{1}{h}\frac{d\theta}{ds} &= 2\kappa + \frac{\Delta\rho g}{\gamma}hz - \frac{\sin(\theta)}{hr}, \\ \frac{d\theta}{ds} &= 2\kappa h + \frac{\Delta\rho g h^2}{\gamma}z - \frac{\sin(\theta)}{r}, \\ \frac{d\theta}{ds} &= \alpha + B_0 z - \frac{\sin(\theta)}{r}, \end{aligned} \tag{9}$$

where $B_0 = \frac{\Delta\rho g h^2}{\gamma}$ is the Bond number, and $\alpha = 2\kappa h$.

Non-dimensionalisation of equation (4)

After introducing the non-dimensional variables and making use of the chain rule we find

$$\begin{aligned}\frac{dV}{dS} &= \pi R^2 \sin(\theta),\\ \frac{dUv}{ds}\frac{ds}{d(hs)} &= \pi (hr)^2 \sin(\theta),\\ \frac{U}{h}\frac{dv}{ds} &= \pi (hr)^2 \sin(\theta),\\ \frac{dv}{ds} &= \frac{\pi h^3}{U} r^2 \sin\theta,\end{aligned}$$

and choosing $U = \pi h^3$, we obtain

$$\frac{dv}{ds} = r^2 \sin\theta. \tag{10}$$

Boundary conditions

In terms of the new variables, the boundary conditions can be written as

$$r(0) = 0, \quad z(0) = 0, \quad \theta(0) = 0, \quad v(0) = 0. \tag{11}$$

The equations are now dimensionless, and the number of parameters has been reduced from five to two. The two remaining parameters are both dimensionless. The Bond number is representative of the ratio between the gravitational and surface tension forces, while α is the ratio between the height of the droplet and the radius of the spherical cap that approximates the droplet shape.

7 Comparison between theory and experiment

By using MATLAB's ode45 function, which is a function that solves a system of differential equations, the non-dimensional system (7) - (10), together with boundary conditions (11) can be solved and plotted together with the experimental data. In order to compare the theoretical and experimental results, we apply a horizontal translation to the experimental data, and both horizontal and vertical translations to the theoretical data so that in both cases the origin is at the bottom centre of the droplet. When observing Figure 6, given that the points represent experimental data while the curve represents the theoretical fit, we see that the theoretical equations fit remarkably well, especially towards the apex of the droplet.

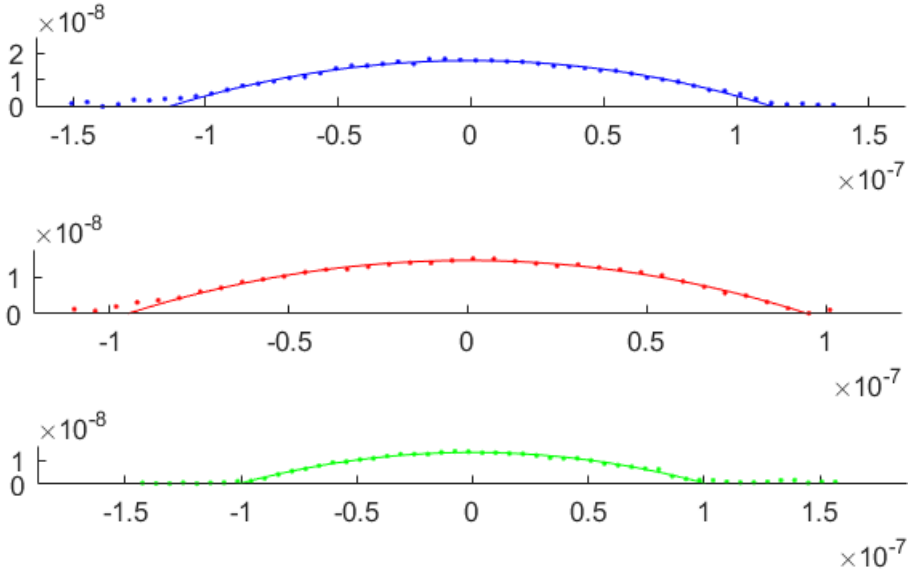

Figure 6: Theoretical results (solid lines) plotted together with the experimental data.

Here we quantitatively compare the theoretical and experimental results in two ways, that is, using the absolute error and the relative error. These two methods share an identical first step which is to calculate theoretical value, y_{theory}, at each data point using linear interpolation. Note that the ode45 solution is not evaluated at the experimental data points and usual MATLAB functions can't be used because the theoretical x coordinate is also a dependent variable. Therefore, these must be calculated manually as follows.

1. For each experimental data point (x_i,y_i), find the two closest theoretical data points $(j, j+1)$ in terms of the horizontal axis such that the experimental point is horizontally in between theoretical points j and $j+1$.

2. Calculate the slope between theoretical points j and $j+1$,

$$m = \frac{z_{j+1} - z_j}{r_{j+1} - r_j}.$$

3. Using the slope, calculate the equation of the straight line between the two theoretical data points,

$$\frac{y_{theory} - z_j}{r - r_j} = m,$$

so that the theoretical prediction of the droplet height, y_{theory}, at the horizontal location of the experimental data point, x_i, is given by

$$y_{theory} = m(x_i - r_j)) + z_j.$$

7.1 Absolute error

Absolute error is the absolute value of the difference between the predicted droplet height and the experimental droplet height,

$$E_{abs} = |y_i - y_{theory}|.$$

The absolute errors between all three data sets and their corresponding theoretical results are plotted together in Figure 7.

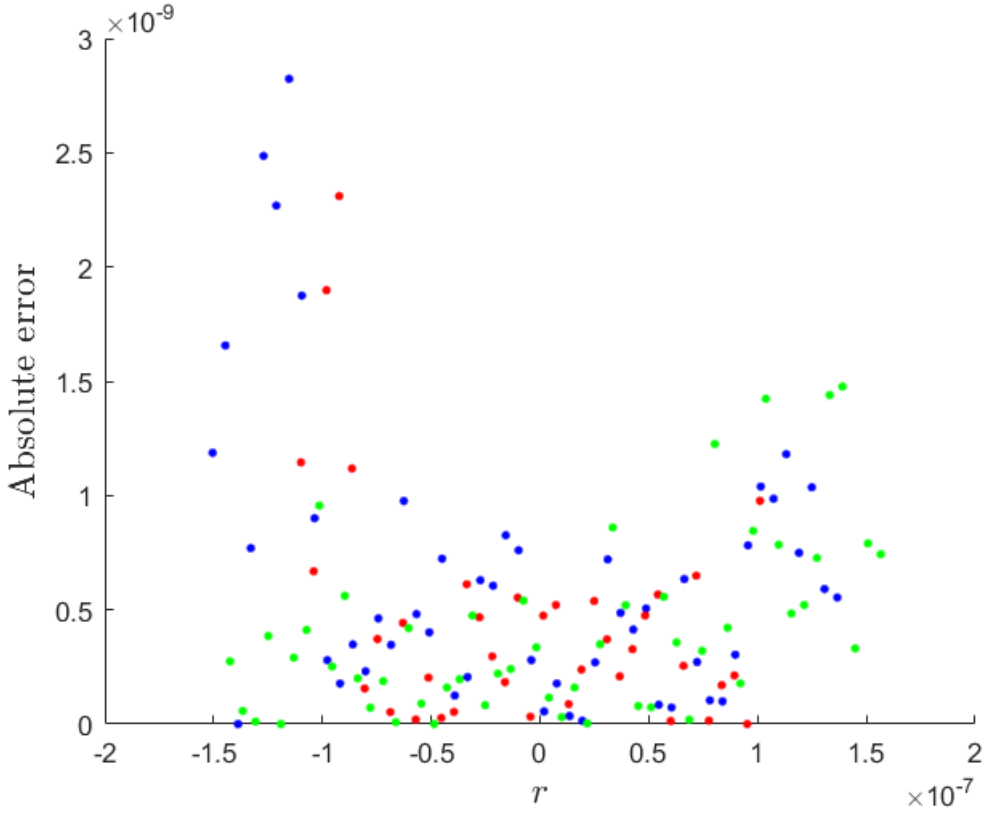

Figure 7: Absolute error between the experimental droplet profiles and the theoretical predictions.

In all three droplet profiles, the errors are larger near the edges of the droplet where the droplet height is comparable to the radius of the AFM tip. As expected, the errors are larger on one side of each droplet than the other. This indicates that the droplets are indeed measured to be steeper on one side than the other due to the angle of the AFM cantilever. Also note that the errors are significantly lower near the apex of the droplet, as anticipated.

7.2 Relative error

The relative error is the ratio between the absolute error and the theoretical prediction. It can identify if the error is large or small in comparison to its size. The formula for the relative error is simply the formula for the

absolute value divided by y_{theory},

$$E_{rel} = \frac{|y_i - y_{theory}|}{y_{theory}}.$$

The relative errors for all three data sets and their corresponding theoretical results are plotted together in Figure 8.

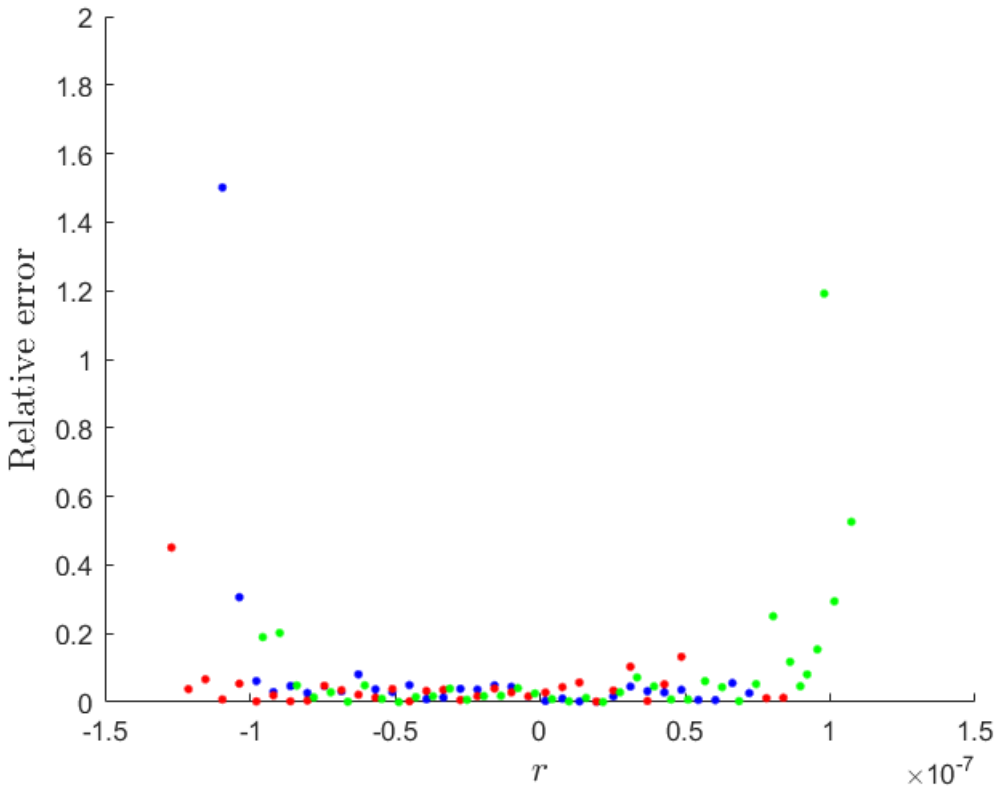

Figure 8: Relative error between the experimental droplet profiles and the theoretical predictions.

The relative error highlights the observations made using the absolute error calculations. The experimental measurements near the centre of the droplet are much more accurate than these near the edges. In addition, since the theoretically predicted profiles are symmetric, this figure clearly shows that the experimental profiles are not symmetric due to the angle of the cantilever.

8 Conclusion

We have quantitatively shown that the experimental errors are greater near the edges of the droplet where the droplet height is comparable to the radius of the AFM tip. In addition, the experimental profiles were shown to be asymmetric due to the angle of the AFM cantilever. The Young-Laplace model and the code developed here can be used to determine both the true shape of nano-scale sessile droplets near their edge and the associated

contact angle.

To improve this work, further investigation could be done to determine a more appropriate way to choose the data used to calculate the curvature at the apex of the droplet. Here, we have used all the data points that lie higher than $\frac{1}{4}$ of the maximum height of the droplet, however this was chosen somewhat arbitrarily and thus its choice could be improved upon.

References

[1] Adamson, A. and Gast, A., 1997. Physical Chemistry Of Surfaces. 6th ed. New York: Wiley.

[2] Krasowska, M., Niecikowska, A. and Beattie, D., 2014. Challenges in imaging of soft layers and structures at solid surfaces using atomic force microscopy. Surface Innovations, 2(3), pp.151-159.

[3] Berg, J., Weber, C. and Riegler, H., 2010. Impact of Negative Line Tension on the Shape of Nanometer-Size Sessile Droplets. Physical Review Letters, 105(7).

[4] Checco, A., Guenoun, P. and Daillant, J., 2003. Nonlinear Dependence of the Contact Angle of Nanodroplets on Contact Line Curvature. Physical Review Letters, 91(18).

[5] Berry, Neeson, Dagastine, Chan, Tabor, 2015. Measurement of surface and interfacial tension using pendant drop tensiometry.

[6] Rotenberg, Boruvka, Neumann, 1983. Determination of Surface Tension and Contact Angle from the Shapes of Axisymmetry Fluid Interfaces.

[7] Rio, Neumann, 1997. Axisymmetric Drop Shape Analysis: Computational Methods for the Measurement of Interfacial Properties from the Shape and Dimensions of Pendant and Sessile Drops.